

# Metamaterials that learn to change shape

Yao Du<sup>1</sup>, Jonas Veenstra<sup>1</sup>, Ryan van Mastrigt<sup>1,2,3</sup>, and Corentin Coulais<sup>1,\*</sup>

<sup>1</sup> *Institute of Physics, University of Amsterdam,*

*Science Park 904, 1098 XH, Amsterdam, The Netherlands*

<sup>2</sup> *AMOLF, Science Park 104, 1098 XG Amsterdam, The Netherlands*

<sup>3</sup> *Gulliver UMR CNRS 7083, ESPCI Paris, PSL University, 10 rue Vauquelin, 75005 Paris, France*

(Dated: January 22, 2025)

Learning to change shape is a fundamental strategy of adaptation and evolution of living organisms, from bacteria and cells to tissues and animals. Human-made materials can also exhibit advanced shape morphing capabilities, but lack the ability to learn. Here, we build metamaterials that can learn complex shape-changing responses using a contrastive learning scheme. By being shown examples of the target shape changes, our metamaterials are able to learn those shape changes by progressively updating internal learning degrees of freedom—the local stiffnesses. Unlike traditional materials that are designed once and for all, our metamaterials have the ability to forget and learn new shape changes in sequence, to learn multiple shape changes that break reciprocity, and to learn multistable shape changes, which in turn allows them to perform reflex gripping actions and locomotion. Our findings establish metamaterials as an exciting platform for physical learning, which in turn opens avenues for the use of physical learning to design adaptive materials and robots.

*Introduction* — One of the distinctive functionalities of living materials, such as biological polymers, cells, tissues, and living organisms is the ability to change shape. A frontier of material science is to create synthetic materials that emulate these shape-changing capabilities. Over the past years, metamaterials have emerged as a prominent platform to do so all the way from the micron [1, 2] to the centimeter [3–16] and meter scale [15, 17–20]. These metamaterials may impact a range of applications from biomedicine [1, 12, 16], robotics [1, 2, 7, 13, 20] and architecture [17, 19–21]. Yet, these shape-morphing metamaterials miss a crucial property that is prevalent in living materials: the ability to adapt their shape-changing response to changing conditions and to learn by modifying their components locally after fabrication [22–25].

Here, inspired by recent developments in physical learning [26–36], we create metamaterials that learn to change shape. The general framework of physical learning aims to emulate nature’s ability to learn in physical systems by systematically adjusting a system’s internal parameters (the so-called learning degrees of freedom) using a predefined local learning rule, thereby evolving the system towards a desired response. Trained under a supervised physical learning scheme, our metamaterials can learn, forget, relearn new shape changes on demand, and even learn multiple target shapes simultaneously. Notably, our learning scheme generalizes to energy non-conserving cases, viz., with nonreciprocity [36–39], and nonlinear cases, viz., with multistability [15, 17, 39]. Taken together, these learned nonreciprocal and multistable shape changes endow our metamaterials with robotic functionalities such as reflex gripping and locomotion. Our study demonstrates that metamaterials are a powerful platform for physical learning and paves the

way toward adaptive materials and robots.

*Experimental setup* — We construct a robotic metamaterial made from  $N$  units consisting of motorized hinges able to exert a torque, the units are connected by an elastic skeleton [Fig. 1(a), see Methods and Supplementary Information for details]. Additionally, each unit has a microcontroller that measures its own angular deflections  $\delta\theta_i$  and exchanges information with its nearest neighbors, stores memory of their past deformations and applies programmable torques via a local feedback loop. These capabilities allow us to adjust the local stiffness of units as we see fit and to implement a torque on each unit  $i$  as

$$\begin{aligned} \tau_i = & - (k_i^o + k^e) \delta\theta_i \\ & - (k_{i-1}^p + k_{i-1}^a) \delta\theta_{i-1} - (k_i^p - k_i^a) \delta\theta_{i+1}, \end{aligned} \quad (1)$$

where  $k_i^o$ ,  $k_i^p$  and  $k_i^a$  are the on-site stiffness, the passive (symmetric) neighbor stiffness, and the active (antisymmetric) neighbor stiffness. These parameters can be manipulated via the local active feedback loop.  $k^e$  is the stiffness of the elastic skeleton and is fixed. We conduct our experiments on a low-friction air table on which the metamaterial can freely move. We apply external deformations by manually fastening some of the units with screws. Doing so generates a torque through the elastic skeleton and active control [Eq. (1)] so that the metamaterial evolves towards a new mechanical equilibrium. In what follows, we aim to control this mechanical equilibrium as a function of the imposed external deformations. We will first consider reciprocal interactions ( $k_i^a = 0$ ) and then generalize our findings to path-dependent nonreciprocal scenarios ( $k_i^a \neq 0$ ).

*Contrastive learning scheme* — To control the shape changes of our metamaterial, we apply a form of physical learning called contrastive learning [27]. Contrastive learning uses the difference between two states of mechanical equilibrium, the free and clamped states, to define a local learning rule. In the free state, only input deformations are imposed. In the clamped state, both

\* coulais@uva.nl

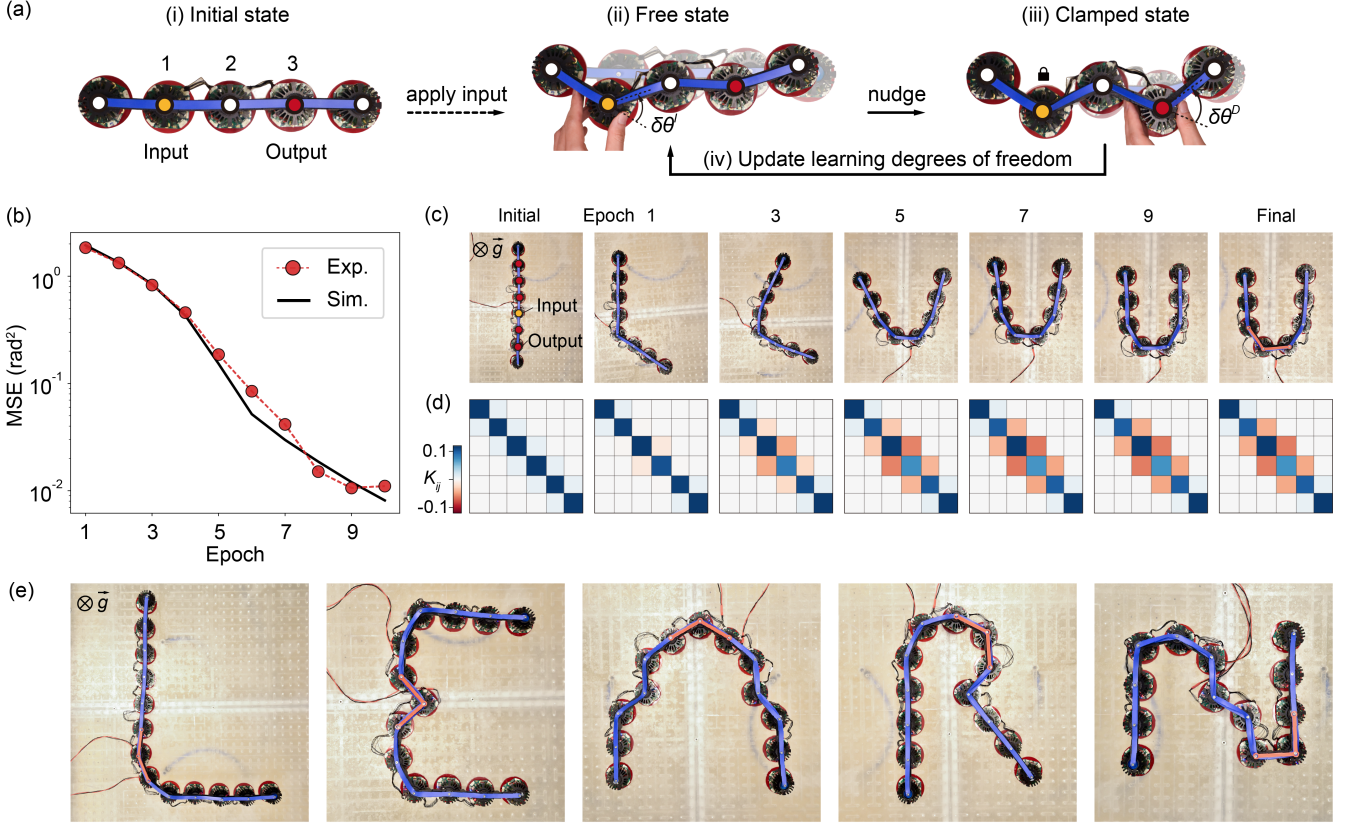


FIG. 1. **Contrastive learning for shape-changing metamaterials.** (a) Contrastive learning scheme. In the free state, the system is deformed from its initial equilibrium state by the input angle  $\delta\theta^I$ , whereas in the clamped state, both the input  $\delta\theta^I$  and the desired output  $\delta\theta^D$  are kept fixed. During learning, steps (ii-iv) are repeated while the learning degrees of freedom are updated according to the contrastive learning rule (See Methods) until a predetermined number of epochs is reached. (b) The MSE curve in simulation (solid line) and experiment (red dots) where a  $N = 6$  robotic chain is trained to morph into a U-shape. Here, the learning rate is  $\gamma = 0.01$ . (c) Equilibrium configurations of each epoch in the free state. Note that the two edge units are not actuated. (d) The stiffness matrix  $K$  during learning. The initial parameters are  $k_i^o = 0.1$ ,  $k_i^p = 0.01$  and  $k_i^a = 0$ . Note  $k^e$  is a constant and thus not shown. (e) A metamaterial with  $N = 11$  is sequentially trained to form the word “LEARN”. See Fig. 5 for the corresponding MSE curves. The red linkage applies the input angular deflection.

input and desired output deformations are imposed simultaneously. The goal is to adjust learning degrees of freedom to achieve the desired output deformations when imposing a predefined input deformation.

In our system, the angular deflections  $\delta\theta_i$  are the so-called physical degrees of freedom: variables that follow from the physical laws governing the system. The tunable stiffnesses  $k_i^o$ ,  $k_i^p$  and  $k_i^a$  are the learning degrees of freedom: parameters that can be tuned and, crucially, influence the resulting physical degrees of freedom. We aim to find an optimal set of stiffnesses that achieves the desired angular deflection  $\delta\theta^D$  for the output units by applying a predefined angular deflection  $\delta\theta^I$  to the input units. Consequently, our metamaterials can morph into a given shape with certain input angular deflections.

To find these stiffnesses that correspond to a desired shape change, we train our metamaterials following a supervised learning protocol [Fig. 1(a)].

(i) Initialization. We set the straight chain as the refer-

ence configuration, i.e.,  $\delta\theta_i = 0$  for all  $i$ . We determine the initial  $k_i^o$  and  $k_i^p$  but set  $k_i^a = 0$ , resulting in a symmetric stiffness matrix  $K$ .

- (ii) We apply fixed input angles  $\delta\theta_i^I$ . The current equilibrium configuration—the free state—is memorized in the microcontroller of each unit.
- (iii) While keeping the input units fixed, we clamp the output units to the desired angle  $\delta\theta_i^D$  and store the new equilibrium configuration—the clamped state.
- (iv) The units compute new stiffnesses using the following local learning rule [Eqs. (4) and (5)] and then update the parameters by a gradient descent step.

The learning protocol consists of repeating steps (ii-iv) within multiple epochs. The local learning rule follows from the gradient of the difference between the function  $\psi(\{\delta\theta\}, \{k\})$  evaluated in the free (F) and clamped (C)

states:

$$\frac{dk_i}{dt} = -\gamma \frac{\partial}{\partial k_i} (\psi^F - \psi^C), \quad (2)$$

where  $\gamma$  is the learning rate and the superscript denotes in which state the function is evaluated. If the metamaterial is passive, i.e.,  $k_i^a = 0$ , its forces derive from a scalar potential. For such a system,  $\psi$  is the elastic energy:

$$\psi = \sum_{i=1}^N \frac{1}{2} (k_i^o + k^e) (\delta\theta_i)^2 + \sum_{i=1}^{N-1} k_i^p \delta\theta_i \delta\theta_{i+1}, \quad (3)$$

where the first term represents the on-site energy of each unit and the second term captures the interaction energy between neighboring units. We then substitute Eq. (3) into Eq. (2) to obtain an explicit learning rule for the passive metamaterial:

$$\frac{dk_i^o}{dt} = -\frac{\gamma}{2} [(\delta\theta_i^C)^2 - (\delta\theta_i^F)^2], \quad (4)$$

$$\frac{dk_i^p}{dt} = -\gamma (\delta\theta_i^C \delta\theta_{i+1}^C - \delta\theta_i^F \delta\theta_{i+1}^F), \quad (5)$$

where  $\delta\theta_i^F$  and  $\delta\theta_i^C$  are the angular deflections of the  $i^{\text{th}}$  unit in the free and clamped states respectively. Note that this learning rule is local because it involves only the angles of unit  $i$  and neighboring unit  $i + 1$ . Employing such a local learning rule over a central one as used in, e.g., back-propagation, requires only local flow of information and is therefore scalable.

*Learning to change shape* — We first demonstrate the learning procedure with a metamaterial with  $N = 6$  units. Our metamaterial learns to form the letter “U” starting from a straight chain when applying an input of  $\delta\theta_3 = \pi/3$ . Here, all other units are outputs. In the free state, we apply only the input in each epoch. In the clamped state, we nudge the chain to the desired shape by fastening the output units in addition to the input units. Using the angular deflections in these two states, each robotic unit calculates  $dk_i/dt$  [Eqs. (4) and (5)] and subsequently updates all  $k_i$ .

During the entire learning procedure (Video 1), the mean square error  $\text{MSE} = \sum_i (\delta\theta_i^F - \delta\theta_i^C)^2 / N_O$  gradually decreases and reaches values below 1% after just 10 iterations in both the simulation and the experiment [Fig. 1(b)]. Here,  $N_O$  is the number of output units. As expected, this coincides with the metamaterial progressively converging to the desired “U” shape in the free state [Fig. 1(c)] and an evolving stiffness matrix [Fig. 1(d)]. In this matrix, the nearest-neighbor stiffnesses  $k_i^p$  evolve towards lower values and become increasingly negative at sites with larger angular deflections. These negative values counteract the natural decay of deformations that occur as a result of the passive elastic skeleton (see Supplementary Information).

To further challenge our metamaterial, we use a longer chain of  $N = 11$  and learn to form all the letters of

the word “LEARN” sequentially as shown in Fig. 1(e) and Video 1. Crucially, our metamaterial can forget the previous shape change and learn the next one without requiring reinitialization.

So far, our metamaterial has been able to learn different shape changes sequentially. What would it take to instead learn multiple shapes all at once? In the following, we will show that implementing an extra physical learning rule to evolve non-reciprocal interactions  $k_i^a$  allows our metamaterials to learn multiple shape changes.

*Non-reciprocal learning rule* — A non-reciprocal mechanical system eludes the Maxwell-Betti theorem, which stipulates that the transmission of forces into displacements is symmetric with respect to the point of application of the load [36–39]. For linear non-reciprocity, the forces do not derive from an energy potential and instead depend on the loading path. If we naively use the elastic energy [Eq. 3] as the function  $\psi$ , the anti-symmetric terms proportional to  $k_i^a$  are canceled out and do not appear in the learning rule (see Methods).

To generalize contrastive learning to non-reciprocal systems, we define a new learning rule that takes into account the path-dependence of the anti-symmetric term  $k_i^a$ . To this end, we introduce a path-dependent work instead of the elastic energy as the function  $\psi$ :

$$\begin{aligned} \psi = & \sum_{i=1}^N \frac{1}{2} (k_i^o + k^e) (\delta\theta_i)^2 \\ & + \sum_{i=1}^{N-1} (k_i^p \delta\theta_i \delta\theta_{i+1} + \alpha_i k_i^a \delta\theta_i \delta\theta_{i+1}). \end{aligned} \quad (6)$$

Here,  $\alpha_i = \text{sgn}(i - I)$  indicates the direction of the loading path between unit  $i$  and an input unit  $I$  (see Methods). If the  $i^{\text{th}}$  unit is on the right side of the input  $I$  ( $i > I$ ), the loading path goes from left to right,  $\alpha_i = 1$  and the contribution to  $\psi$  by  $k_i^a$  is positive. In contrast, if the  $i^{\text{th}}$  unit is on the left side of the input  $I$  ( $i < I$ ), the loading path goes backward from right to left,  $\alpha_i = -1$  and the contribution to  $\psi$  by  $k_i^a$  is negative. Substituting Eq. (6) into Eq. (2), we obtain the updated values for each stiffness component. The explicit learning rules of  $k_i^o$  and  $k_i^p$  remain the same as Eqs. (4) and (5), but that of  $k_i^a$  is

$$\frac{dk_i^a}{dt} = -\alpha_i \gamma (\delta\theta_i^C \delta\theta_{i+1}^C - \delta\theta_i^F \delta\theta_{i+1}^F). \quad (7)$$

Now, equipped with this path-dependent learning rule, we next apply it to our metamaterials to learn non-reciprocal responses.

*Non-reciprocal shape changes* — We return to the metamaterial with  $N = 6$  units and train it to learn the non-reciprocal shape changes depicted in Fig. 2(a). Specifically, applying a positive curvature to unit 2 leads to a positive curvature to unit 5, whereas applying a positive curvature to unit 5 leads to a negative curvature to unit 2. If one tries to learn this response with a reciprocal metamaterial ( $k_i^a = 0$ ,  $p$  configuration), it

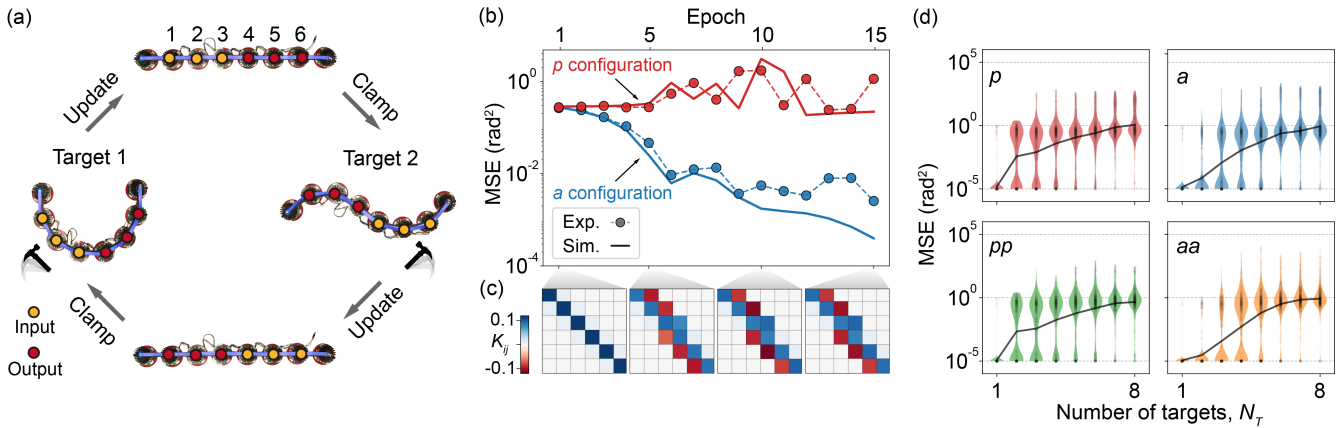


FIG. 2. **Learning non-reciprocal shape changes and multiple targets.** (a) The procedure of learning non-reciprocal shape changes. Each target shape is learned following the above protocol in Fig. 1(a) but the learning is conducted by switching between these two targets in turn during each epoch. (b) The MSE curves of learning the above non-reciprocal shape changes in the  $p$  configuration (red) and the  $a$  configuration (blue) show that these targets can only be learned simultaneously with non-reciprocal interactions, i.e., in the  $a$  configuration. Due to human operation error and the precision limitation of the experimental setup, the experimental MSE deviates slightly from the simulated curve after 10 epochs. (c) The stiffness matrix  $K$  of the metamaterial in the  $a$  configuration during learning. The initial parameters are  $k_i^o = 0.1$ ,  $k_i^p = 0.01$  and  $k_i^a = 0$ . The learning rate is  $\gamma = 0.05$ . (d) Simulation results of learning multiple targets with (non)reciprocal, and next nearest neighbor interactions ( $p$ ,  $a$ ,  $pp$  and  $aa$ ). A system of  $N = 10$  is simulated and the number of targets  $N_T$  varied from 1 to 8. The black semi-transparent dots are the MSE of each simulation and each column consists of 500 simulations. The solid line is the average MSE. The cut-off of the MSE is arbitrarily chosen to be  $10^{-5} \text{ rad}^2$ .

fails [Fig. 2(b)], whereas in a nonreciprocal metamaterial ( $k_i^a \neq 0$ ,  $a$  configuration), the learning is successful (Video 2). This means non-reciprocity is essential for generating shape changes that break the symmetry between loading directions. As learning proceeds, we note that the stiffness matrix of the non-reciprocal metamaterial, which was initially symmetric, gradually becomes asymmetric [Fig. 2(c)]. Thus, we can train a reciprocal metamaterial to become non-reciprocal. Such non-reciprocal learning is distinct from all earlier studies on contrastive learning, which only consider reciprocal systems [27, 28, 34, 35].

*Multi-target learning* — Non-reciprocity enables the metamaterial to learn multiple shape changes, even if these are not compatible according to the Maxwell-Betti theorem. The question is what sets the maximum number of shape changes? To answer this question, we systematically learn multiple targets for a  $N = 10$  metamaterial and compare reciprocal and non-reciprocal cases. We denote the number of targets as  $N_T$ . Here, each target consists of a single randomly selected input unit and a single randomly selected output unit. Similar to Fig. 2(a), our metamaterial learns these targets in sequence during each epoch to generate all desired shape changes. Our metamaterial performs poorly once the number of targets exceeds one ( $N_T > 1$ ) in the  $p$  configuration [Fig. 2(d)]. This is because two distinct shape changes likely break the Maxwell-Betti relation. In contrast, upon introducing  $k_i^a$  (the  $a$  configuration) the metamaterial learns well up to  $N_T = 3$ .

To further increase the number of targets the meta-

material can learn, we consider scenarios in which the unit cells can also communicate with their next nearest neighbors—we refer to these configurations as  $pp$  and  $aa$  for the reciprocal and non-reciprocal cases (see Methods). Whereas the  $pp$  configuration does not bring an appreciable improvement, the  $aa$  configuration can learn up to  $N_T = 4$ . The fact that a larger learning space enables more complex learning tasks is consistent with earlier studies [40–42] and can be rationalized by a basic constraint counting argument (see Supplementary Information). Besides increasing the number of learning degrees of freedom, a straightforward strategy to address this limited learning capacity is to increase the number of units (see Supplementary Information). To illustrate the ability of our metamaterials to learn four multiple targets we train our metamaterial to deform into the letters “LEREN” (Dutch for “LEARN”) upon application of the appropriate input deformation (Video 2). In contrast to Fig. 1(e), there is no retraining, the four letters are learned simultaneously, and the metamaterial can generate all four shapes depending on the angles and locations of the input units.

*Multistable shape changes* — So far, our metamaterials have been trained in monostable scenarios: they spring back to the initial flat configuration once the input units are released. Surprisingly, by playing with our metamaterials, we discover that our metamaterials can have multistable configurations [Fig. 3(a) and Video 3]. To understand where this unexpected multistability comes from, we start with a pair of units and analyze its stability. Its linear stability is determined by the eigenvalues of

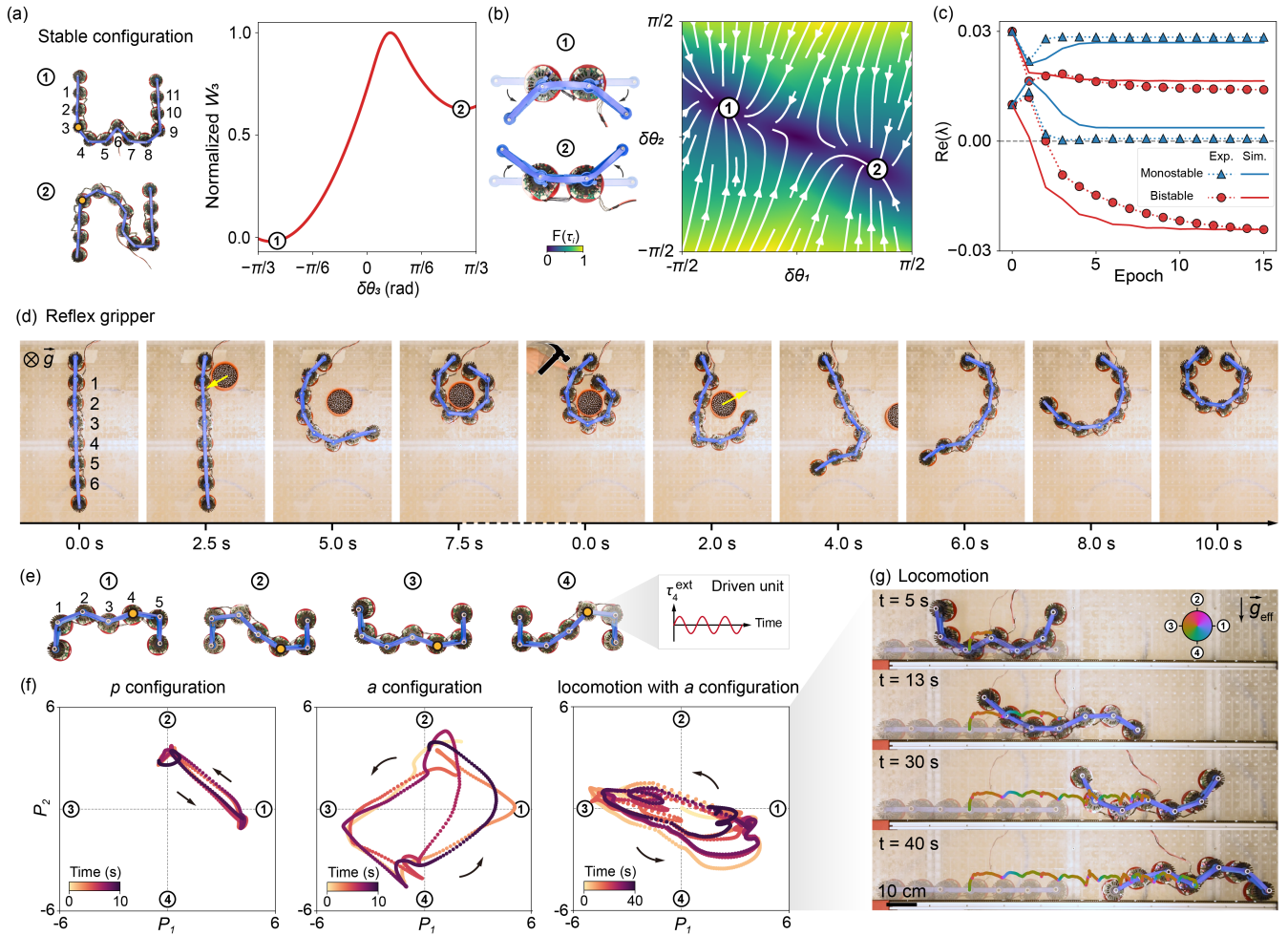


**FIG. 3. Learning multistable shape changes and robotic functionalities** (a) The normalized work landscape of unit 3 (yellow dot) by tuning  $\delta\theta_3$ . Two local minima correspond to two stable configurations, the letters “W” and “N”. (b) A pair of units show bistable behavior. The flat configuration corresponds to the zero deformations. Upon perturbation, the system jumps to a non-zero deformation instead of springing back to the initial configuration. The left inset shows the two stable configurations. The right inset shows the force fields of the bistable case in which two stable fixed points exist. The colorbar shows the normalized total torque  $F(\tau_i) = \sqrt{\tau_1^2 + \tau_2^2}/F_{\max}$ . (c) The real part of the eigenvalues  $\lambda$  during learning for a pair of unit in both monostable and bistable scenarios that learn the same target. The desired shape change is generating  $\delta\theta_2 = -\pi/6$  rad after applying  $\delta\theta_1 = \pi/6$  rad. The imaginary part is zero so it is not shown here. (d) A metamaterial with  $N = 6$  is trained as a reflex gripper (See Video 3). It can automatically catch a moving object and release it when an input is applied. (e-g) Using a trained metamaterial with non-reciprocal interactions to achieve locomotion (See Video 3). (e) The metamaterial with  $N = 5$  initially learns to generate the letter “M” (shape 1) and has four stable shapes. The system is driven by applying an external sine torque  $\tau_4^{\text{ext}}$  on unit 4 (yellow dot). (f) The deformation of the system over time with the  $p$ ,  $a$  configuration and when it locomotes with the  $a$  configuration. Data plotted in shape space projected onto the two vectors ( $P_1$ ,  $P_2$ ) (See Methods) and colored with time. (g) Snapshots of the locomotion and the trajectory of the center of mass colored by the angle of the projected shape  $P_1 + iP_2$ . With the airtable inclined under an angle, gravity  $\vec{g}_{\text{eff}}$  points downwards.

the stiffness matrix  $K$  (see Supplementary Information). The system is unstable if there is at least one negative real eigenvalue. Such negative eigenvalues are made possible by the tunable stiffnesses  $k_i^o$ ,  $k_i^p$  and  $k_i^a$  which, unlike the stiffness of the elastic skeleton, need not be positive. Therefore the stiffness matrix need not be positive definite. When one eigenvalue is negative, the deformations amplify exponentially. This amplification is balanced by the limited maximum torque that the motors can apply

and the restoring torque from the elastic skeleton. As a result, when the flat configuration is no longer stable, two stable deformed configurations emerge [Fig. 3(b)].

This unexpected discovery triggers a fascinating question: how can we learn multistable shape changes? To achieve this, we introduce a local stability constraint to our contrastive learning scheme based on the Gershgorin circle theorem [43] (see Methods). In addition, a gradient descent term is added in Eq. (4), whose modified version

takes the form

$$\frac{dk_i^o}{dt} = -\frac{\gamma}{2} \left[ (\delta\theta_i^C)^2 - (\delta\theta_i^F)^2 \right] - 2\gamma(k_i^o - k^*). \quad (8)$$

Here,  $k^*$  is a predetermined value that allows us to tune the stability of the metamaterial. For  $k^* < -k^e$  ( $k^* > -k^e$ ), the metamaterial will learn an unstable (stable) shape change provided  $|k^* + k^e| > |k_{i-1}^p + k_{i-1}^a| + |k_i^p - k_i^a|$  for any  $i$  (for all  $i$ ) (see Methods). Crucially, this constrained learning rule is local and can be implemented with contrastive learning. To prove its feasibility, we use this pair of units and train it to generate the same desired shape changes but with different stability [Fig. 3(c)]. The eigenvalues always remain positive in the monostable case while one negative eigenvalue emerges in the bistable case.

Next, we apply this principle to larger metamaterials to achieve robotic functionalities. In Fig. 3(d) and Video 3, we build a reflex gripper that can automatically catch an object once it touches the gripper. Furthermore, the gripper can also release the object and kick it away by pushing unit 1. This is because  $k_1^o$  is negative and unit 1 is bistable. Finally, we use a multistable robotic chain to achieve locomotion. The robotic chain is initially trained to generate the letter “M”. In order to trigger multistability,  $k_2^o$  and  $k_4^o$  are trained to be negative, so that there are four stable configurations as shown in Fig. 3(e). Surprisingly, the metamaterial exhibits a cyclic shape shift when a sine external torque is applied in a single driven unit [Fig. 3(f) and Video 3]—whereas such cycles are usually achieved with two motors driven with a constant phase

delay [44–47]. As a result, the metamaterial can locomote on a substrate [Fig. 3(g) and Video 3]. We note that such cyclic shape change only occurs when the interactions are non-reciprocal ( $a$  configuration,  $k_i^a \neq 0$ ). Thus, we have shown that periodically driving a single unit generates cycles through shape space by combining multistability [48, 49] and nonreciprocity [37, 45, 47, 50] which leads to a stable locomotion gait.

*Conclusion and Outlook* — In conclusion, we have constructed metamaterials that can learn, forget, and relearn to change shape by leveraging a local physical learning strategy. They can do so with multiple shapes, in a non-reciprocal fashion, exhibit multiple stable configurations, and achieve robotic functionalities. Our work paves avenues for the design of adaptive metamaterials [51, 52], and soft and distributed robotics [46, 53–55]. An exciting question ahead is how to extend physical learning to dynamical [36, 37, 56] and stochastic scenarios and to mimic the autonomous and adaptive behavior of living matter.

## ACKNOWLEDGMENTS

We thank M. Stern, V. Vitelli, A. Liu, D. Durian, J. Schwarz and S. Dillavou for the insightful discussions and suggestions and K. van Nieuwland, D. Giesen, R. Hassing and S. Koot for technical assistance. Y. D. acknowledges financial support from the China Scholarship Council. We acknowledge funding from the European Research Council under Grant Agreement No. 852587 and from the Netherlands Organisation for Scientific Research (NWO) under grant agreement VIDI 2131313.

- 
- [1] C. L. Smart, T. G. Pearson, Z. Liang, M. X. Lim, M. I. Abdelrahman, F. Monticone, I. Cohen, and P. L. McEuen, Magnetically programmed diffractive robotics, *Science* **386**, 1031 (2024).
  - [2] Q. Liu, W. Wang, H. Sinhmar, I. Griniasty, J. Z. Kim, J. T. Pelster, P. Chaudhari, M. F. Reynolds, M. C. Cao, D. A. Muller, A. B. Apsel, N. L. Abbott, H. Kress-Gazit, P. L. McEuen, and I. Cohen, Electronically configurable microscopic metasheet robots, *Nature Materials* **24**, 109 (2025).
  - [3] J. L. Silverberg, J.-H. Na, A. A. Evans, B. Liu, T. C. Hull, C. Santangelo, R. J. Lang, R. C. Hayward, and I. Cohen, Origami structures with a critical transition to bistability arising from hidden degrees of freedom, *Nature Materials* **14**, 389 (2015).
  - [4] C. Coulais, E. Teomy, K. de Reus, Y. Shokef, and M. van Hecke, Combinatorial design of textured mechanical metamaterials, *Nature* **535**, 529 (2016).
  - [5] J. T. B. Overvelde, J. C. Weaver, C. Hoberman, and K. Bertoldi, Rational design of reconfigurable prismatic architected materials, *Nature* **541**, 347 (2017).
  - [6] Y. Kim, H. Yuk, R. Zhao, S. A. Chester, and X. Zhao, Printing ferromagnetic domains for untethered fast-transforming soft materials, *Nature* **558**, 274 (2018).
  - [7] A. Rafsanjani, Y. Zhang, B. Liu, S. M. Rubinstein, and K. Bertoldi, Kirigami skins make a simple soft actuator crawl, *Science Robotics* **3**, eaar7555 (2018).
  - [8] E. Siéfert, E. Reyssat, J. Bico, and B. Roman, Bio-inspired pneumatic shape-morphing elastomers, *Nature Materials* **18**, 24 (2019).
  - [9] G. P. T. Choi, L. H. Dudte, and L. Mahadevan, Programming shape using kirigami tessellations, *Nature Materials* **18**, 999 (2019).
  - [10] A. Zareei, B. Deng, and K. Bertoldi, Harnessing transition waves to realize deployable structures, *Proceedings of the National Academy of Sciences* **117**, 4015 (2020).
  - [11] L. Jin, A. E. Forte, B. Deng, A. Rafsanjani, and K. Bertoldi, Kirigami-Inspired Inflatables with Programmable Shapes, *Advanced Materials* **32**, 2001863 (2020).
  - [12] T. Van Manen, S. Janbaz, K. M. B. Jansen, and A. A. Zadpoor, 4D printing of reconfigurable metamaterials and devices, *Communications Materials* **2**, 56 (2021).
  - [13] D. Hwang, E. J. Barron, A. B. M. T. Haque, and M. D. Bartlett, Shape morphing mechanical metamaterials through reversible plasticity, *Science Robotics* **7**,

- eabg2171 (2022).
- [14] T. Gao, J. Bico, and B. Roman, Pneumatic cells toward absolute Gaussian morphing, *Science* **381**, 862 (2023).
  - [15] A. S. Meeussen and M. Van Hecke, Multistable sheets with rewritable patterns for switchable shape-morphing, *Nature* **621**, 516 (2023).
  - [16] M. T. Flavin, K.-H. Ha, Z. Guo, S. Li, J.-T. Kim, T. Saxena, D. Simatos, F. Al-Najjar, Y. Mao, S. Bandapalli, C. Fan, D. Bai, Z. Zhang, Y. Zhang, E. Flavin, K. E. Madsen, Y. Huang, L. Emu, J. Zhao, J.-Y. Yoo, M. Park, J. Shin, A. G. Huang, H.-S. Shin, J. E. Colgate, Y. Huang, Z. Xie, H. Jiang, and J. A. Rogers, Bioelastic state recovery for haptic sensory substitution, *Nature* **635**, 345 (2024).
  - [17] D. Melancon, B. Gorissen, C. J. García-Mora, C. Hoberman, and K. Bertoldi, Multistable inflatable origami structures at the metre scale, *Nature* **592**, 545 (2021).
  - [18] Y. Ren, J. Panetta, S. Suzuki, U. Kusupati, F. Isvoranu, and M. Pauly, Computational Homogenization for Inverse Design of Surface-based Inflatables, *ACM Transactions on Graphics* **43**, 1 (2024).
  - [19] L. Stein-Montalvo, L. Ding, M. Hultmark, S. Adriaenssens, and E. Bou-Zeid, Kirigami-inspired wind steering for natural ventilation, *Journal of Wind Engineering and Industrial Aerodynamics* **246**, 105667 (2024).
  - [20] Y. Li, A. Di Lallo, J. Zhu, Y. Chi, H. Su, and J. Yin, Adaptive hierarchical origami-based metastructures, *Nature Communications* **15**, 6247 (2024).
  - [21] E. R. Adrover, *Deployable Structures* (Hachette UK, London, 2015).
  - [22] R. Bastien, T. Bohr, B. Moulia, and S. Douady, Unifying a model of shoot gravitropism reveals proprioception as a central feature of posture control in plants, *Proceedings of the National Academy of Sciences* **110**, 755 (2013).
  - [23] L. Talà, A. Fineberg, P. Kukura, and A. Persat, *Pseudomonas aeruginosa* orchestrates twitching motility by sequential control of type IV pili movements, *Nature Microbiology* **4**, 774 (2019).
  - [24] G. Noselli, A. Beran, M. Arroyo, and A. DeSimone, Swimming *Euglena* respond to confinement with a behavioural change enabling effective crawling, *Nature Physics* **15**, 496 (2019).
  - [25] M. Kramar and K. Alim, Encoding memory in tube diameter hierarchy of living flow network, *Proceedings of the National Academy of Sciences* **118**, e2007815118 (2021).
  - [26] N. Pashine, D. Hexner, A. J. Liu, and S. R. Nagel, Directed aging, memory, and nature's greed, *Science Advances* **5**, eaax4215 (2019).
  - [27] M. Stern, D. Hexner, J. W. Rocks, and A. J. Liu, Supervised Learning in Physical Networks: From Machine Learning to Learning Machines, *Physical Review X* **11**, 021045 (2021).
  - [28] S. Dillavou, M. Stern, A. J. Liu, and D. J. Durian, Demonstration of Decentralized Physics-Driven Learning, *Physical Review Applied* **18**, 014040 (2022).
  - [29] M. Stern and A. Murugan, Learning Without Neurons in Physical Systems, *Annual Review of Condensed Matter Physics* **14**, 417 (2023).
  - [30] M. J. Falk, J. Wu, A. Matthews, V. Sachdeva, N. Pashine, M. L. Gardel, S. R. Nagel, and A. Murugan, Learning to learn by using nonequilibrium training protocols for adaptable materials, *Proceedings of the National Academy of Sciences* **120**, e2219558120 (2023).
  - [31] M. Falk, A. Strupp, B. Scellier, and A. Murugan, Contrastive learning through non-equilibrium memory (2023), arXiv:2312.17723.
  - [32] V. P. Patil, I. Ho, and M. Prakash, Self-learning mechanical circuits (2023), arXiv:2304.08711.
  - [33] C. G. Evans, J. O'Brien, E. Winfree, and A. Murugan, Pattern recognition in the nucleation kinetics of non-equilibrium self-assembly, *Nature* **625**, 500 (2024).
  - [34] L. E. Altman, M. Stern, A. J. Liu, and D. J. Durian, Experimental demonstration of coupled learning in elastic networks, *Physical Review Applied* **22**, 024053 (2024).
  - [35] S. Dillavou, B. D. Beyer, M. Stern, A. J. Liu, M. Z. Miskin, and D. J. Durian, Machine learning without a processor: Emergent learning in a nonlinear analog network, *Proceedings of the National Academy of Sciences* **121**, e2319718121 (2024).
  - [36] R. Mandal, R. Huang, M. Fruchart, P. G. Moerman, S. Vaikuntanathan, A. Murugan, and V. Vitelli, Learning dynamical behaviors in physical systems (2024), arXiv:2406.07856.
  - [37] M. Brandenbourger, C. Scheibner, J. Veenstra, V. Vitelli, and C. Coulais, Limit cycles turn active matter into robots (2022), arXiv:2108.08837.
  - [38] M. Fruchart, C. Scheibner, and V. Vitelli, Odd Viscosity and Odd Elasticity, *Annual Review of Condensed Matter Physics* **14**, 471 (2023).
  - [39] J. Veenstra, O. Gamayun, X. Guo, A. Sarvi, C. V. Meinersen, and C. Coulais, Non-reciprocal topological solitons in active metamaterials, *Nature* **627**, 528 (2024).
  - [40] J. W. Rocks, H. Ronellenfisch, A. J. Liu, S. R. Nagel, and E. Katifori, Limits of multifunctionality in tunable networks, *Proceedings of the National Academy of Sciences* **116**, 2506 (2019).
  - [41] M. Stern, M. B. Pinson, and A. Murugan, Continual Learning of Multiple Memories in Mechanical Networks, *Physical Review X* **10**, 031044 (2020).
  - [42] M. Stern, M. Guzman, F. Martins, A. J. Liu, and V. Balasubramanian, Physical networks become what they learn (2024), arXiv:2406.09689.
  - [43] G. Semyon Aronovich, Über die Abgrenzung der Eigenwerte einer Matrix, *Bulletin de l'Académie des Sciences de l'URSS*, 749 (1931).
  - [44] A. J. Ijspeert, A. Crespi, D. Ryczko, and J.-M. Cabelguen, From Swimming to Walking with a Salamander Robot Driven by a Spinal Cord Model, *Science* **315**, 1416 (2007).
  - [45] W. Savoie, T. A. Berrueta, Z. Jackson, A. Pervan, R. Warkentin, S. Li, T. D. Murphey, K. Wiesenfeld, and D. I. Goldman, A robot made of robots: Emergent transport and control of a smarticle ensemble, *Science Robotics* **4**, eaax4316 (2019).
  - [46] G. Oliveri, L. C. van Laake, C. Carissimo, C. Miette, and J. T. B. Overvelde, Continuous learning of emergent behavior in robotic matter, *Proceedings of the National Academy of Sciences* **118**, e2017015118 (2021).
  - [47] S. Li, T. Wang, V. H. Kojouharov, J. McInerney, E. Aydin, Y. Ozkan-Aydin, D. I. Goldman, and D. Z. Rocklin, Robotic swimming in curved space via geometric phase, *Proceedings of the National Academy of Sciences* **119**, e2200924119 (2022).
  - [48] M. Van Hecke, Profusion of transition pathways for interacting hysterons, *Physical Review E* **104**, 054608 (2021).
  - [49] P. Baconnier, M. H. Teunisse, and M. v. Hecke, Proliferation and prevention of self-loops in ensembles of inter-

- [acting binary elements](#) (2024), arXiv:2412.12658.
- [50] E. M. Purcell, Life at low Reynolds number, *American Journal of Physics* **45**, 3 (1977).
  - [51] R. H. Lee, E. A. B. Mulder, and J. B. Hopkins, Mechanical neural networks: Architected materials that learn behaviors, *Science Robotics* , **10** (2022).
  - [52] G. Bordiga, E. Medina, S. Jafarzadeh, C. Bösch, R. P. Adams, V. Tournat, and K. Bertoldi, Automated discovery of reprogrammable nonlinear dynamic metamaterials, *Nature Materials* **23**, 1486 (2024).
  - [53] S. Li, R. Batra, D. Brown, H.-D. Chang, N. Ranganathan, C. Hoberman, D. Rus, and H. Lipson, Particle robotics based on statistical mechanics of loosely coupled components, *Nature* **567**, 361 (2019).
  - [54] B. Saintyves, M. Spenko, and H. M. Jaeger, A self-organizing robotic aggregate using solid and liquid-like collective states, *Science Robotics* **9**, eadh4130 (2024).
  - [55] S. Zou, S. Picella, J. De Vries, V. G. Kortman, A. Sakes, and J. T. B. Overvelde, A retrofit sensing strategy for soft fluidic robots, *Nature Communications* **15**, 539 (2024).
  - [56] C. Klos, Y. F. Kalle Kossio, S. Goedeke, A. Gilra, and R.-M. Memmesheimer, Dynamical Learning of Dynamics, *Physical Review Letters* **125**, 088103 (2020).

## METHODS

### A. Experimental setup

Our robotic metamaterials are made of multiple robotic units composed of motorized vertices connected by 3D printed plastic arms and an elastic skeleton with stiffness  $k^e = 12\text{mN} \cdot \text{m}/\text{rad}$  (Fig. 4). Each vertex con-

sists of a DC coreless motor (Motraxx CL1628) embedded in a cylindrical heatsink, an angular encoder (CUI AMT113S), and a microcontroller (ESP32) connected to a custom electronic board. The electronic board enables power conversion, interfaces the sensor and motor, and enables communication between vertices. The motor is able to produce an external torque based on Eq. (1). We note that the motor will saturate at a maximum torque of  $\tau_{max} = 12\text{mN} \cdot \text{m}$  in practice, so each robotic unit follows a nonlinear force function:

$$\tau_i = \begin{cases} (k_{i-1}^p + k_{i-1}^a) \delta\theta_{i-1} - k_i^o \delta\theta_i - (k_i^p - k_i^a) \delta\theta_{i+1}, & \text{if } |\tau_i| < \tau_{max} \\ \text{sgn}(\tau_i) \tau_{max}, & \text{if } |\tau_i| \geq \tau_{max}. \end{cases} \quad (9)$$

Experiments are conducted on top of a custom-made low-friction air table. Each motorized vertex sits on top of a circular disk that ensures that the robotic unit floats on a thin layer of pressurized air without touching the table (Fig. 4). The experimental pictures are taken from the top view. By fastening the screws on the units, we can apply angular deflections on demand. The units can store their angular deflections, do calculations in the microcontroller, and update their onsite stiffnesses and neighbor interactions at will.

#### 1. Locomotion experiment

In Fig. 3(e-g), the airtable was tilted with respect to the horizontal plane. This induces an effective gravity  $\vec{g}_{\text{eff}}$  pointing toward a treadmill. The frequency of the sinusoidal forcing is 0.25 Hz. The deformation is plotted in the space of two main deformation vectors,  $P_1$  and  $P_2$  defined as

$$\begin{aligned} P_1 &= \delta\Theta \cdot \frac{\mathbf{v}_1}{\|\mathbf{v}_1\|}, \\ P_2 &= \delta\Theta \cdot \frac{\mathbf{v}_2}{\|\mathbf{v}_2\|}. \end{aligned} \quad (10)$$

Here,  $\delta\Theta$  is the angular deflection vector. We define  $\mathbf{v}_1 = \{1, 1, -1, 1, 1\}^\top$  and  $\mathbf{v}_2 = \{1, 1, 0, -1, -1\}^\top$  to correspond to the shapes of letter ‘‘M’’ and letter ‘‘N’’ respectively in Fig. 3(e).

### B. Simulation protocol

In contrastive learning [27], a physical system is trained by observing the contrast between its ‘‘free state’’ and ‘‘clamped state’’. For our robotic metamaterials, this procedure follows four steps as shown in Fig. 1(a), which we now describe in more detail.

*Initialization* — We set the initial configuration to be flat and ensure that the initial onsite and neighbor in-

teractions are such that the system is monostable (see Sec. E). The input and desired output angular deflection vectors are  $\delta\Theta^I$  and  $\delta\Theta^D$  of size  $N$ . The sets of input and output indices are  $\mathcal{I}$  and  $\mathcal{D}$ . For example, for a system with  $N = 3$ , if the learning task is to achieve a desired output  $\delta\theta_3^D$  once an input  $\delta\theta_1^I$  is applied [Fig. 1(a)], then we have  $\delta\Theta^I = \{\delta\theta_1^I, 0, 0\}^\top$ ,  $\delta\Theta^D = \{0, 0, \delta\theta_3^D\}^\top$ ,  $\mathcal{I} = \{1\}^\top$  and  $\mathcal{D} = \{3\}^\top$ .

*Free state* — After applying the input angles  $\delta\Theta^I$ , we calculate the induced torque on each unit  $\tau_i^F$  which is given by

$$\tau_i^F = - \sum_{j=1}^N K_{ij} \delta\theta_j^I. \quad (11)$$

Then, we find the angle vector  $\delta\Theta^F$  corresponding mechanical equilibrium, i.e.,  $\tau_i = 0$  for  $i \notin \mathcal{I}$ , by inverting the stiffness matrix  $K$ . The resulting state is called the free state and reads

$$\delta\theta_i^F = \begin{cases} - \sum_{j=1}^N (K^{-1})_{ij} \tau_j^F, & \text{if } i \notin \mathcal{I} \\ \delta\theta_i^I, & \text{if } i \in \mathcal{I}. \end{cases} \quad (12)$$

*Clamped state* — We now determine the nudging angle vector  $\delta\Theta^N$  with entries

$$\delta\theta_i^N = \begin{cases} \delta\theta_i^F, & \text{if } i \notin \mathcal{D} \\ \delta\theta_i^D, & \text{if } i \in \mathcal{D}, \end{cases} \quad (13)$$

and find the torque on each unit  $\tau_i^C$  induced when the system is clamped at the nudging angle  $\delta\Theta^N$

$$\tau_i^C = - \sum_{j=1}^N K_{ij} \delta\theta_j^N. \quad (14)$$

We now find the equilibrium configuration of the clamped state given by the angle vector  $\delta\Theta^C$ , whose en-

tries read

$$\delta\theta_i^C = \begin{cases} -\sum_{j=1}^N K_{ij}^{-1} \tau_j^C, & \text{if } i \notin (\mathcal{I} \cup \mathcal{D}) \\ \delta\theta_i^N, & \text{if } i \in (\mathcal{I} \cup \mathcal{D}). \end{cases} \quad (15)$$

*Updating* — By substituting the angles of the free  $\delta\Theta^F$  and clamped states  $\delta\Theta^C$  into Eqs. (4), (5) and (7), we update the stiffness matrix  $K$ . The above operation will be repeated for a number of epochs. The learning error is defined by the mean squared error (MSE):

$$\text{MSE} = \frac{1}{N_O} \sum_{i \in \mathcal{D}} (\delta\theta_i^F - \delta\theta_i^D)^2, \quad (16)$$

where  $N_O$  is the number of output units. The simulation code is available at <https://github.com/YaoDu001/Metamaterials-that-learn-shape-changes.git>.

### C. Contrastive learning rule

In an earlier study [27], contrastive learning was applied to passive, reciprocal systems, using a learning rule derived from the elastic energy difference between the free and clamped states. If we consider a system described by Eq. (1), its elastic energy  $E$  takes the following form:

$$\begin{aligned} E &= -\frac{1}{2} \delta\Theta^\top K \delta\Theta \\ &= -\frac{1}{2} \sum_{i=1}^N (k_i^o + k^e) (\delta\theta_i)^2 - \sum_{i=1}^{N-1} k_i^p \delta\theta_i \delta\theta_{i+1}. \end{aligned} \quad (17)$$

Here, we can see that the active stiffness  $k_i^a$  does not contribute to the total elastic energy. It means the elastic energy cannot be used solely to inform an update rule if we intend to update  $k_i^a$ .

To generalize contrastive learning to non-reciprocal systems, we use path-dependent work  $\psi$  as shown in Eq. (6). We now derive this new path-dependent learning rule. We consider a 2-unit system as an example, its constitutive relation is

$$\begin{pmatrix} \tau_1 \\ \tau_2 \end{pmatrix} = - \begin{bmatrix} k_1^o + k^e & k_1^p - k_1^a \\ k_1^p + k_1^a & k_2^o + k^e \end{bmatrix} \begin{pmatrix} \delta\theta_1 \\ \delta\theta_2 \end{pmatrix}. \quad (18)$$

Let us consider training unit 2 to deform in response to an input deflection of unit 1 as  $\delta\theta_1^I \rightarrow \delta\theta_1^D$ . To learn this response, we first apply  $\delta\theta_1^I$ , and allow the system to reach the corresponding free state, given by mechanical equilibrium. The work done to reach the free state is called  $W_{1 \rightarrow 2}^F$ . We then clamp the system by nudging  $\delta\theta_2$  to its desired response  $\delta\theta_2^D$  while keeping  $\delta\theta_1$  fixed. The work done by nudging system to the clamped state from the free state is referred to  $\Delta W_{1 \rightarrow 2}$  and the work to achieve the clamped state from the initial configuration is referred to as  $W_{1 \rightarrow 2}^C$ . We assume the loading is applied

quasistatically and that the instantaneous torque is the only force that does work when the system equilibrates to free or clamped states. Explicitly, the above terms are

$$W_{1 \rightarrow 2}^F = \int_0^{\delta\theta_1^F} \tau_1 d\delta\theta_1 + \int_0^{\delta\theta_2^F} \tau_2 d\delta\theta_2, \quad (19)$$

$$W_{1 \rightarrow 2}^C = \int_0^{\delta\theta_1^C} \tau_1 d\delta\theta_1 + \int_0^{\delta\theta_2^C} \tau_2 d\delta\theta_2, \quad (20)$$

$$\Delta W_{1 \rightarrow 2} = \int_{\delta\theta_1^F}^{\delta\theta_1^C} \tau_1 d\delta\theta_1 + \int_{\delta\theta_2^F}^{\delta\theta_2^C} \tau_2 d\delta\theta_2. \quad (21)$$

$W_{1 \rightarrow 2}^F$  is easy to evaluate since  $\tau_2 = 0$  and only  $\tau_1$  does work in the free state, but  $W_{1 \rightarrow 2}^C$  cannot be derived directly because both  $\tau_1$  and  $\tau_2$  do work and are functions of  $\delta\theta_1$  and  $\delta\theta_2$ . Fortunately, we can easily calculate the work difference  $\Delta W_{1 \rightarrow 2}$  since  $\delta\theta_1^F = \delta\theta_1^C$ , such that Eq. (21) simplifies to

$$\begin{aligned} \Delta W_{1 \rightarrow 2} &= \int_{\delta\theta_2^F}^{\delta\theta_2^C} \tau_2 d\delta\theta_2 \\ &= \int_{\delta\theta_2^F}^{\delta\theta_2^C} [-(k_1^p + k_1^a) \delta\theta_1^F - (k_2^o + k^e) \delta\theta_2] d\delta\theta_2 \\ &= -\frac{1}{2} (k_2^o + k^e) [(\delta\theta_2^C)^2 - (\delta\theta_2^F)^2] \\ &\quad - (k_1^p + k_1^a) (\delta\theta_1^C \delta\theta_2^C - \delta\theta_1^F \delta\theta_2^F). \end{aligned} \quad (22)$$

Conversely, if we intend to learn a target as  $\delta\theta_2^I \rightarrow \delta\theta_1^D$ , the work difference  $\Delta W_{2 \rightarrow 1}$  equals

$$\Delta W_{2 \rightarrow 1} = \int_{\delta\theta_1^F}^{\delta\theta_1^C} \tau_1 d\delta\theta_1 + \int_{\delta\theta_2^F}^{\delta\theta_2^C} \tau_2 d\delta\theta_2. \quad (23)$$

Since  $\delta\theta_2^F = \delta\theta_2^C$ , Eq. (23) simplifies to

$$\begin{aligned} \Delta W_{2 \rightarrow 1} &= \int_{\delta\theta_1^F}^{\delta\theta_1^C} \tau_1 d\delta\theta_1 \\ &= \int_{\delta\theta_1^F}^{\delta\theta_1^C} [-(k_1^o + k^e) \delta\theta_1 - (k_1^p - k_1^a) \delta\theta_2^F] d\delta\theta_1 \\ &= -\frac{1}{2} (k_1^o + k^e) [(\delta\theta_1^C)^2 - (\delta\theta_1^F)^2] \\ &\quad - (k_1^p - k_1^a) (\delta\theta_1^C \delta\theta_2^C - \delta\theta_1^F \delta\theta_2^F). \end{aligned} \quad (24)$$

Comparing Eqs. (22) and (24), we can see the contribution of  $k_i^a$  is path dependent. We combine Eqs. (22) and (24) and now define  $\Delta W$  as the path-dependent work difference between the free state and the clamped state. In this case,  $\Delta W$  equals

$$\begin{aligned} \Delta W &= -\frac{1}{2} (k_1^o + k^e) [(\delta\theta_1^C)^2 - (\delta\theta_1^F)^2] \\ &\quad - (k_1^p + \alpha k_1^a) (\delta\theta_1^C \delta\theta_2^C - \delta\theta_1^F \delta\theta_2^F). \end{aligned} \quad (25)$$

Here,  $\alpha = \pm 1$  indicates the direction of the loading path. For the learning targets  $\delta\theta_1^I \rightarrow \delta\theta_2^D$  and  $\delta\theta_2^I \rightarrow \delta\theta_1^D$ , the loading paths are unit 1  $\rightarrow$  unit 2 and unit 2  $\rightarrow$  unit 1, and  $\alpha = 1$  and  $-1$  respectively.

Subsequently, we generalize the work difference between the free state and the clamped state in a system with  $N$  units as

$$\begin{aligned} \Delta W = & -\frac{1}{2} \sum_{i=1}^N (k_i^o + k^e) [(\delta\theta_i^C)^2 - (\delta\theta_i^F)^2] \\ & - \sum_{i=1}^{N-1} (k_i^p + \alpha_i k_i^a) (\delta\theta_i^C \delta\theta_{i+1}^C - \delta\theta_i^F \delta\theta_{i+1}^F). \end{aligned} \quad (26)$$

Here,  $\alpha_i = \text{sgn}(i-I)$  indicates the direction of the loading path between unit  $i$  and an input unit  $I$ . Note that  $I$  can be any one of the input unit indices. If  $i > I$ , i.e., the  $i^{\text{th}}$  unit is on the right side of the input  $I$ , the loading path goes from left to right,  $\alpha_i = 1$  and the contribution to  $\Delta W$  by  $k_i^a$  is positive. In contrast, if  $i < I$ , i.e., the  $i^{\text{th}}$  unit is on the left side of the input  $I$ , the loading path goes backward from right to left,  $\alpha_i = -1$  and the contribution to  $\psi$  by  $k_i^a$  is negative.

We directly replace  $\psi^F - \psi^C$  in Eq. (2) by  $\Delta W$  [Eq. (26)] and interpret Eq. (6) as a path-dependent work. Thus, we obtain the explicit local learning rules for our non-reciprocal system as shown in Eqs. (4), (5) and (7).

#### D. System with the second nearest-neighbor interactions

We also consider next nearest-neighbor interactions. With those interactions, each robotic unit  $i$  exerts a torque as follows:

$$\begin{aligned} \tau_i = & -(k_i^o + k^e) \delta\theta_i \\ & - (k_{i-1}^p + k_{i-1}^a) \delta\theta_{i-1} - (k_i^p - k_i^a) \delta\theta_{i+1} \\ & - (k_{i-2}^{pp} + k_{i-2}^{aa}) \delta\theta_{i-2} - (k_{i-2}^{pp} - k_{i-2}^{aa}) \delta\theta_{i+2}, \end{aligned} \quad (27)$$

where  $k_i^{pp}$  and  $k_i^{aa}$  are the passive (symmetric) and active (anti-symmetric) next nearest-neighbor stiffnesses. We refer to the case when  $k_i^a = k_i^{aa} = 0$  as the *pp* configuration. Otherwise, we refer to the *aa* configuration.

The path-dependent work  $\psi$  for the *aa* configuration equals

$$\begin{aligned} \psi = & \sum_{i=1}^N \frac{1}{2} (k_i^o + k^e) (\delta\theta_i)^2 \\ & + \sum_{i=1}^{N-1} (k_i^p \delta\theta_i \delta\theta_{i+1} + \alpha_i k_i^a \delta\theta_i \delta\theta_{i+1}) \\ & + \sum_{i=1}^{N-2} (k_i^{pp} \delta\theta_i \delta\theta_{i+2} + \alpha_i k_i^{aa} \delta\theta_i \delta\theta_{i+2}). \end{aligned} \quad (28)$$

Substituting Eq. (28) into Eq. (2), the learning rules of  $k_i^o$ ,  $k_i^p$  and  $k_i^a$  remain the same as Eqs. (4), (5) and (7), but these of  $k_i^{pp}$  and  $k_i^{aa}$  are

$$\begin{aligned} \frac{dk_i^{pp}}{dt} = & -\gamma (\delta\theta_i^C \delta\theta_{i+2}^C - \delta\theta_i^F \delta\theta_{i+2}^F), \\ \frac{dk_i^{aa}}{dt} = & -\alpha_i \gamma (\delta\theta_i^C \delta\theta_{i+2}^C - \delta\theta_i^F \delta\theta_{i+2}^F). \end{aligned} \quad (29)$$

#### E. Stability constraint in contrastive learning

Our stability constraint rule is based on the Gershgorin circle theorem [43]. For a square  $n \times n$  matrix  $A$ , the theorem states that each eigenvalue of  $A$  lies within at least one of the Gershgorin disks. The center and radius of each Gershgorin disk are simply defined using the information from each row of  $A$ . Let  $R_i$  be the sum of the absolute values of the off-diagonal entries in the  $i^{\text{th}}$  row as  $R_i = \sum_{i \neq j}^n |a_{ij}|$ . A Gershgorin disk  $D(a_{ii}, R_i)$  is defined as a circle with a center of the diagonal entry  $a_{ii}$  and a radius of  $R_i$  in the complex space.

Using the Gershgorin circle theorem, we impose a local constraint on the eigenvalues of the stiffness matrix  $K$ . Considering Eq. (1),  $K$  is a tridiagonal matrix, we have that  $R_i = |k_{i-1}^p + k_{i-1}^a| + |k_i^p - k_i^a|$  and  $a_{ii} = k_i^o + k^e$ . According to the stability analysis (see Supplementary Information), to ensure the system is monostable without negative real eigenvalues, the following stability constraint must be imposed during contrastive learning:

$$\begin{cases} k_i^o + k^e > 0, & \forall i \\ R_i < |k_i^o + k^e|, & \forall i. \end{cases} \quad (30)$$

After each epoch, the stiffnesses stops evolving if any unit violates the above constraint. Eq. (30) makes sure the Gershgorin discs located in the positive real part of the complex space so that all eigenvalues have positive real parts. Conversely, multistability is ensured when there is at least one negative real eigenvalue, i.e., when there is at least one unit  $i$  for which

$$\begin{cases} k_i^o + k^e < 0, \\ R_i < |k_i^o + k^e|. \end{cases} \quad (31)$$

With this stability constraint, we can now trigger multistability during contrastive learning. To do this, we impose an extra gradient descent [Eq. (8)] on a set of units  $\mathcal{M}$  thus push their on-site stiffness  $k^o$  to be negative. This ensures that the units  $i$  in  $\mathcal{M}$  follow the above stability constraint [Eq. (31)] so that negative real eigenvalues appear during learning. We use this constrained learning rule to train multistable metamaterials and demonstrate robotic applications [Fig. 3(d-g) and Video. 3].



FIG. 4. The side view of the robotic unit cells. Each unit cell is a motorized vertex connected by 3D printed plastic arms and elastic rubber bands. It consists of a DC motor embedded in a cylindrical heatsink and a microcontroller connected to a custom electronic board. The electronic board enables communication between vertices. Each motorized vertex sits on top of a red circular disk that ensures that the robotic unit floats on the air table. We apply external deformations by manually fastening the screws.

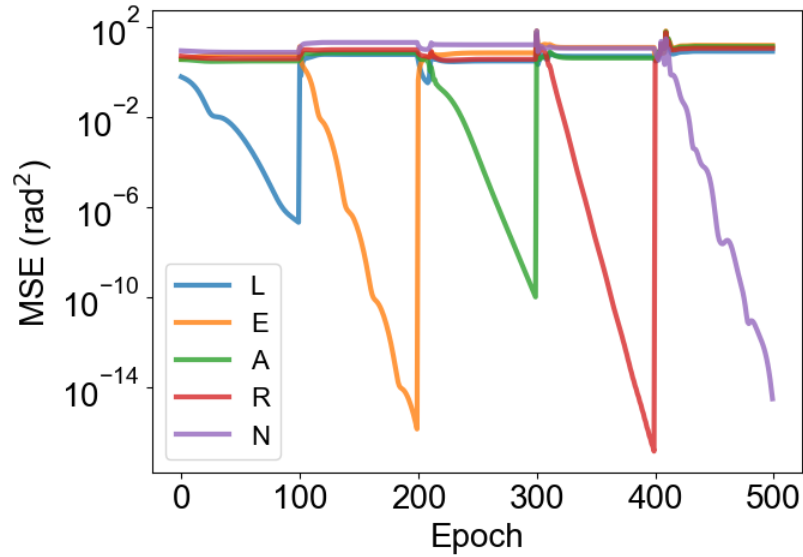


FIG. 5. The MSE curves of the metamaterial with  $N = 11$  learns to form the word “LEARN” sequentially in Fig. 1(e). The curves show that our metamaterial can forget the previous shape change and relearn the next one without requiring reinitialization. Here, the learning is conducted in simulation and the learning rate is  $\gamma = 0.001$ . The initial parameters are  $k_i^o = 0.1$ ,  $k_i^p = 0.01$  and  $k_i^a = 0$ .